NANO LETTERS

pubs.acs.org/NanoLett Letter

Zone-Folded Longitudinal Acoustic Phonons Driving Self-Trapped State Emission in Colloidal CdSe Nanoplatelet Superlattices

Xinyu Sui, Xiaoqing Gao, Xianxin Wu, Chun Li, Xuekang Yang, Wenna Du, Zhengping Ding, Shengye Jin, Kaifeng Wu, Tze Chien Sum, Peng Gao, Junjie Liu, Xiaoding Wei, Jun Zhang, Qing Zhang, Zhiyong Tang,* and Xinfeng Liu*

Cite This: *Nano Lett.* 2021, 21, 4137−4144 Read Online

ACCESS | Metrics & More | Article Recommendations | Supporting Information

ABSTRACT: Colloidal CdSe nanoplatelets (NPLs) have substantial potential in light-emitting applications because of their quantum-well-like characteristics. The self-trapped state (STS), originating from strong electron−phonon coupling (EPC), is promising in white light luminance because of its broadband emission. However, achieving STS in CdSe NPLs is extremely challenging because of their intrinsic weak EPC nature. Herein, we developed a strong STS emission in the spectral range of 450−600 nm by building superlattice (SL) structures with colloidal CdSe NPLs. We demonstrated that STS is generated via strong coupling of excitons and zone-folded longitudinal acoustic phonons with formation time of ∼450 fs and localization length of ∼0.56 nm. The Huang−Rhys factor, describing the EPC strength in SL structure, is estimated to be ∼19.9, which is much larger than that (∼0.1) of monodispersed CdSe NPLs. Our results provide an in-depth understanding of STS and a platform for generating and manipulating STS by designing SL structures.

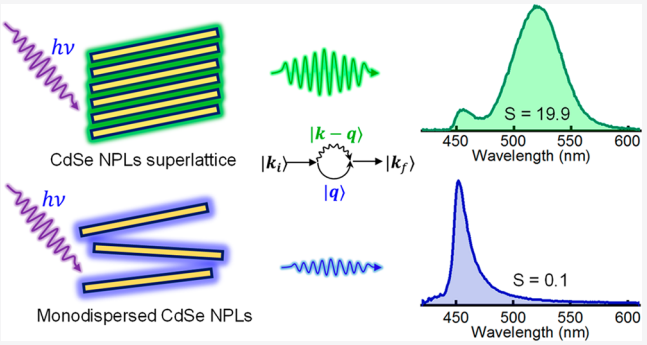

KEYWORDS: *CdSe nanoplatelets, self-trapped state, electron−phonon coupling, superlattices, transient absorption spectroscopy, low-frequency Raman*

INTRODUCTION

Ultrathin colloidal CdX (X = S, Se, Te) nanoplatelets (NPLs) with a uniform atomic thickness form a new class of two-dimensional material.[1−4] They have attracted considerable attention in past decades for their excellent optical properties, such as a narrow line width because of strong quantum thickness confinement,[5,6] a high luminescent quantum yield, and large mode gain coefficients.[7−10] These remarkable optical properties, along with their cost-effective preparation and notable stability, have made colloidal CdX NPLs promising for light-emitting diodes and lasers.[8,11−18] Therefore, manipulating optical transition of elementary excitations and regulating emission behaviors in these NPLs are fundamentally important for their further applications.[19,20]

The self-trapped state (STS) is a localized carrier state trapped by deformation potential from surrounding lattices with strong electron−phonon coupling (EPC).[21] STS has been widely observed in various condensed matters, such as rare gases, alkali halides, lead halides, and organic solids.[22,23] Radiative recombination from STS has typical features, such as large Stokes shift and broad emission bandwidth, which promote its application in one-step white-light illumination and wide gamut display.[24,25] For colloidal CdX NPLs, the realization of STS emission can further extend their optoelectronic application range and promote their "lab-to-fab" transformation. However, the weak EPC nature in a CdX NPL system makes it challenging to create STS.[26,27] One possible method is to increase the fluctuation of a rigid lattice by reducing the geometric scale of II−VI colloidal nanocrystals into the atom-cluster regime. However, it suffers from its structural stability.[28−32]

To further relax restrictions of the lattice softness, a desirable solution is to construct hybrid superlattice (SL) structures constituted by self-assembly of colloidal nanocrystals with long-range order for their rich phonon dynamics.[33−36] The alternating order of soft organic ligands and rigid inorganic frameworks can be analogous with the periodic bead-spring system, where coherent longitudinal acoustic vibrations are generated from building blocks. These acoustic phonons propagate across the entire SL structure and introduce

Received: October 26, 2020
Revised: April 23, 2021
Published: April 29, 2021

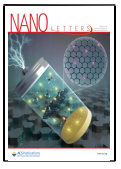

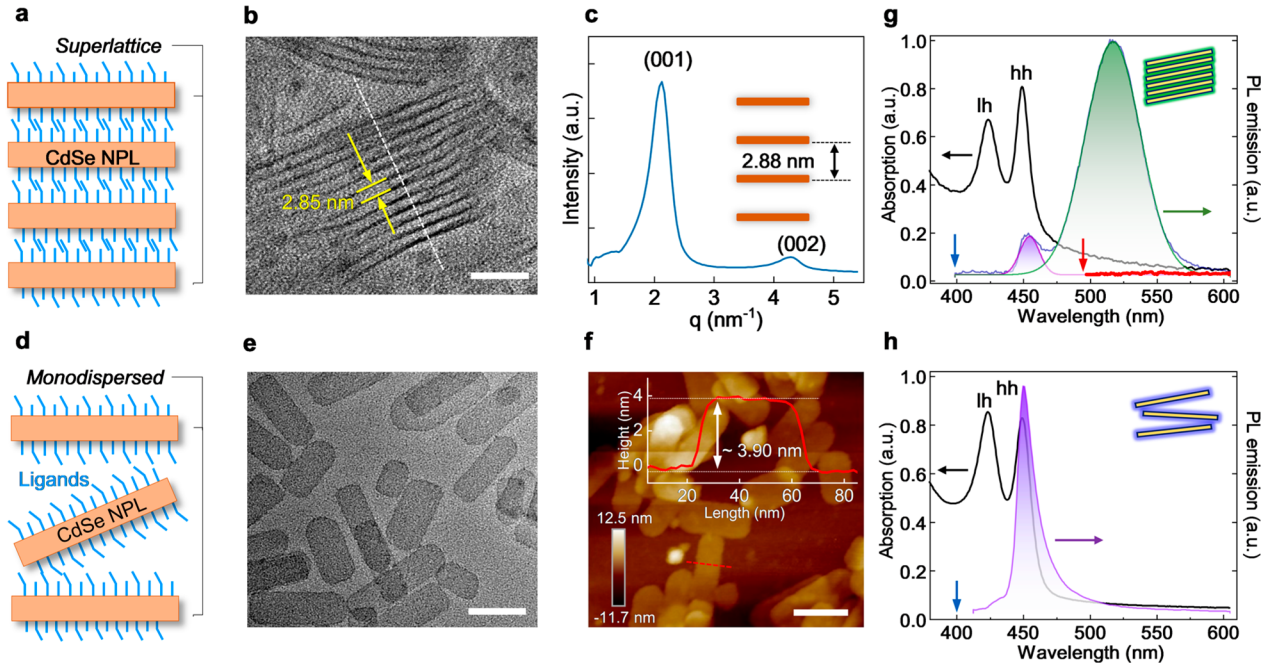

Figure 1. (a) Schematic structure of CdSe NPL SLs. (b) TEM image of CdSe NPL SLs with edge-on orientation. Center-to-center distance is measured to be ~2.85 nm. Scale bar is 20 nm. (c) Small-angle X-ray scattering pattern of CdSe NPL SLs. The first and second scattering peaks with scattering wave vector **q** of 2.17 and 4.35 nm^{-1}, corresponding to a SL structure period of ~2.88 nm. (d) Schematic of monodispersed CdSe NPLs. (e) TEM image of monodispersed CdSe NPLs with face-on orientation. Scale bar is 100 nm. (f) AFM image of monodispersed CdSe NPLs on SiO_2 substrate. Scale bar is 100 nm. Average height is ~3.90 nm along the red-dashed section line. (g) Room-temperature absorption and PL spectra of CdSe NPL SLs. Two-peak emission is observed excited by CW laser of 400 nm (marked with blue arrow). Indistinguishable emission (red line) is excited by a CW laser of 485 nm (marked with red arrow). (h) Room-temperature absorption and PL spectra of monodispersed CdSe NPLs. The emission is excited by a CW laser of 400 nm (marked with blue arrow).

additional lattice deformation compared with individual units. Coherent longitudinal acoustic phonons have been reported in various hybrid SLs of silver and gold nanocrytstals,[37,38] cobalt nanocrystals,[39,40] CdSe nanocrystals, and two-dimensional perovskites.[41,42] In principle, it is feasible to use the collective acoustic phonon modes from hybrid SLs to generate STS via strong EPC.

In this study, we demonstrate the strong STS emission in the spectral range of 450−600 nm by building hybrid SL structures of colloidal CdSe NPLs. Through systematic optical spectroscopy studies, we discovered that STS is generated by the strong coupling of excitons and zone-folded longitudinal acoustic phonons (ZFLAPs) in SLs. ZFLAPs are formed by bulk acoustic phonon folding into a mini-Brillouin zone of the SL. We revealed that the STS is formed in a time scale of ~450 fs and localized in a spatial extent of ~0.56 nm. The Huang−Rhys parameter, which describes the EPC strength in SL structure, is estimated to be ~19.9, which is much larger than that (~0.1) of monodispersed CdSe NPL. The in-depth understanding of the STS emission mechanism in this study bears important implications for manipulating STS through optimal design of SL structures.

RESULTS AND DISCUSSION

The SLs of colloidal wurtzite CdSe NPL (see Figure 1a) were synthesized via a modified soft-template procedure and dispersed in toluene as described in a previous study.[43] The thickness of the NPL (regardless of surface ligands, c_0) was controlled to be ~1.41 nm (see Figure S1) with ~3.5 monolayer. Transmission electron microscope (TEM) images (see Figure 1b and Figure S2) of these SLs showed a distinct stacking structure with center-to-center distance, d_0, of ~2.85 nm, which is consistent with the data (~2.88 nm in Figure 1c) measured by small-angle X-ray scattering. However, the thickness (with surface ligands), h_0, of the monodispersed NPLs (Figure 1d,e) is ~3.90 nm (see Figure 1f) characterized by atomic force microscopy (AFM), which is comparable with a previous report.[43] The large differences between d_0 (2.85 nm) and h_0 (3.90 nm) suggest ligands interdigitation of ~1 nm in NPL SLs (see the schematic in Figure S3), implying that the ligands are buckled with each other for 80% of their free length (~1.25 nm).[43] It thus weakens the configurational entropy of ligands and strengthens their van der Waals interactions, promoting a stable SL framework.[36,44]

For CdSe NPL SLs, steady-state absorption spectroscopy at room temperature (black curve, Figure 1g) exhibits two discrete peaks at 426 and 451 nm, representing light-hole exciton transition and heavy-hole exciton transition, respectively.[2] Photoluminescence (PL) spectrum under continuous wave (CW) laser of 400 nm (indicated by blue arrow, Figure 1g) shows two emission bands: an excitonic emission centered at 456 nm with a full width at half-maximum (fwhm) of 75 meV and a lower energy peak at 516 nm with fwhm of 228 meV (fitting details see Figure S4 and Table S1). A below-bandgap excitation observed using CW laser at 485 nm (indicated by the red arrow) shows indistinguishable PL (Figure 1g), suggesting that both 456 and 516 nm emissions share the same excited states. Moreover, during the unbundling process of NPL SLs, the broadband emission centered at 516 nm gradually disappeared (see Figures S5−S7). The monodispersed NPLs exhibit monochromatic excitonic emission centered at 452 nm and an almost unchanged

https://doi.org/10.1021/acs.nanolett.0c04169
Nano Lett. 2021, 21, 4137−4144

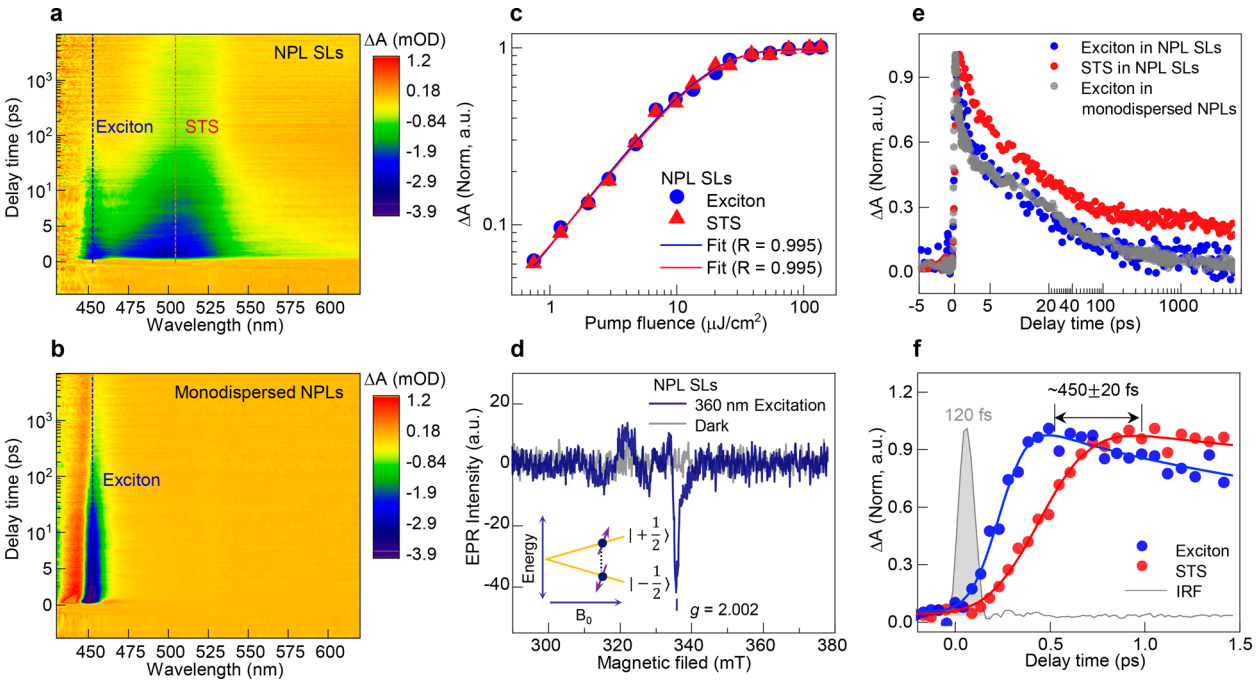

Figure 2. Two-dimensional pseudo color map of the TA profile of (a) CdSe NPL SLs and (b) monodispersed NPLs. (c) Normalized ΔA intensity of exciton (blue) and STS (red) as a function of pump fluence in CdSe NPL SLs. Curves are fitted based on the Poisson distribution model with relative coefficient $R = 0.995$. (d) Photoexcited EPR spectrum of CdSe NPL SLs (dark blue) with g parameter of 2.002 ± 0.001 excited with CW laser of 360 nm. EPR signal with dark condition is plotted in gray. Inset presents an EPR sketch map. (e) Normalized decay dynamics of exciton state and STS from CdSe NPL SLs and monodispersed NPLs, respectively. (f) Difference of onset time between exciton state and STS in CdSe NPL SLs with 450 ± 20 fs. The instrument response function with 120 fs is plotted in gray.

absorption spectrum (Figure 1h). The structure-sensitive emission properties indicate that the broadband emission peak, centered at 516 nm, can be attributed to the STS emission rather than the defect or trap states emission. More experimental data is provided below to confirm the role of STS.

We conducted transient absorption (TA) measurements for both NPL SLs and monodispersed NPLs in toluene solution. Figure 2a,b shows the pseudo color map of differential absorption (ΔA) as a function of delay time with 400 nm excitation (pump fluence of, 2.7 $\mu J/cm^2$). Both NPL SLs and monodispersed NPLs show negative excitonic bleaching at 452 nm. In NPL SLs (Figure 2a), the extra negative peak located at 508 nm stems from STS emission, which is supported by pump-fluence dependent ΔA measurement (see Figure 2c). The nearly identical saturation trends for exciton and STS (after normalization) can be well fitted using a saturation absorption model (details see in Supporting Information Note S1) within the pump fluence range over 2 orders of magnitude (0.77 to 154 $\mu J/cm^2$). This behavior eliminates the identification of defect or trapped states. Other evidence, such as linear power-dependent PL spectrum (see Figure S8), similar PL excitation spectrum with exciton states (see Figure S8), and balanced element distributions in X-ray photoelectron spectroscopy (Figure S9 and Table S2), further strengthen the nature of STS. The observed negative peak at 508 nm for STS in TA spectra is stimulated emission (SE) instead of ground state bleaching.[45] This is because there is no ground state occupation for STS, which is indicated by the negligible PL (Figure 1g) and TA signal (Figure S10) with below-bandgap excitation.

The type of STS as hole self-trapping is verified using photoexcited EPR spectroscopy, as depicted in Figure 2d.[46] The obtained g-factor of 2.002 ± 0.001 for NPL SLs (see details in methods in Supporting Information) is identical to the value of the free electron in vacuum (g_e = 2.002), indicating the trapped hole property according to previous reports (see Table S3).[47] However, no EPR signal was observed (Figure S11) in controlled monodispersed NPL samples. The hole self-trapping behavior can be explained by the large effective mass of the heavy hole ($0.45m_0$) compared to that of electrons ($0.13m_0$).[48]

To explore the forming process of STS, the decay profiles of excitons and STS from TA spectra are normalized in Figure 2e. All dynamics can be fitted via a triexponential decay model (see Supporting Information Note S2 and Figure S12). STS has an average lifetime of ~3.00 ns, which is 8.3 times longer than that of excitons (~0.36 ns, Table S4). The time-resolved PL data indicates the slow recombination processes of STS (see Figure S13) than that of excitons. The typical long lifetime of STS can be attributed to the reduced wave function overlap induced by strong EPC.[25] The normalized onset dynamics of exciton and STS are plotted in Figure 2f. An ultrafast onset time of 450 ± 20 fs is obtained for the STS by comparing the rising edge between STS and exciton. Because STS is localized and stabilized through lattice distortions induced by phonons, the STS formation time is always related to one vibration cycle of phonon.[49−52] Although other processes, such as electron−electron and electron−phonon scattering, can also contribute to the STS formation, they can be negligible because their time scales are significantly longer than 450 fs.[53−55] Considering that the formation time of STS is known (450 fs), we can estimate the phonon energy Ω_p as 9.2 meV (or 74 cm^{-1}) through the time-energy uncertainty relation of $\Omega_p = \hbar/\tau$. This phonon is located in the energy range of acoustic phonon branch in bulk CdSe crystal.[56]

https://doi.org/10.1021/acs.nanolett.0c04169
Nano Lett. 2021, 21, 4137−4144

The observation of coherent phonons upon photoexcitation in TA spectra facilitates the investigation of transient EPC dynamics in STS (see details Supporting Information Note S3).[57] From the first 9 ps delay in the TA spectra for CdSe NPL SLs, the strong oscillations originating from coherent phonons are observed over time in the STS SE region between 475 and 580 nm (Figure 3a). Figure 3b demonstrated the ΔA

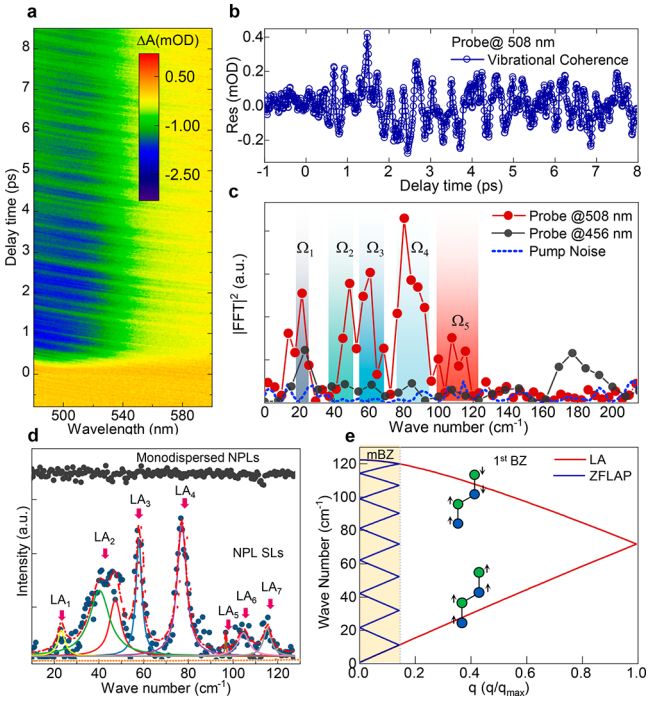

Figure 3. (a) Contour plot TA spectra of CdSe NPL SLs in the first 9 ps delay window. (b) Oscillatory components probed at 508 nm as the residual part are extracted by subtracting the population decay background. (c) FFT power spectrum of the oscillatory components probed at 508 nm (STS) and 456 nm (exciton state). A native noise background from laser power fluctuation is plotted in gray. (d) Raman spectroscopy of monodispersed CdSe NPLs and CdSe NPL SLs. Raman signals from NPL SLs are fitted via multi-Lorentz peaks. Sum of the overall fitting is plotted as a red-dashed line. A set of peaks are labeled as LA_1−LA_7. (e) Calculated ZFLAP dispersion in colloidal CdSe NPL SLs in mini-Brillouin zone (labeled as mBZ) is filled with yellow. The longitudinal acoustic phonon dispersion of the CdSe crystal in the first Brillouin zone is indicated by the red line. Inset presents the lattice vibrational diagram for upper and lower acoustic phonon branch.

oscillation component probed at 508 nm (belongs to STS) following population background subtraction. The corresponding frequencies of the coherent phonons determined by fast Fourier transform (FFT) are presented in Figure 3c. The noise spectrum from the pump laser is provided as a baseline (see details in Figure S14). A set of vibrational frequencies are observed and indexed with $\Omega_1 \approx 22$ cm^{-1}, $\Omega_2 \approx 48$ cm^{-1}, $\Omega_3 \approx 62$ cm^{-1}, $\Omega_4 \approx 80$ cm^{-1}, and $\Omega_5 \approx 115$ cm^{-1}. For comparison, coherent phonons modulated on the exciton state probed at 456 nm (see details in Figure S15) show the vibrational frequencies at 22 and 180 cm^{-1} (Figure 3c). The former (22 cm^{-1}) is similar to Ω_1 in STS, whereas the latter (180 cm^{-1}) belongs to the reported surface optical phonons.[58] Different coherent phonons observed between exciton and STS indicate that Ω_1−Ω_5 are mainly coupled on STS rather than exciton state. For the STS part, time-frequency analysis demonstrates that all of the five modes (Ω_1−Ω_5) work together almost simultaneously (Supporting Information Note S4, Figure S16). Therefore, the mean phonon energy can be estimated to be 65 cm^{-1}, which is comparable to the value of Ω_p (74 cm^{-1}) estimated from the STS onset time. Moreover, the five modes (Ω_1−Ω_5) are not observed from monodispersed NPLs (see Figure S17), indicating that these modes are tightly related to the CdSe NPL SLs structure.

We used low-frequency Raman spectroscopy to further study the origin of these five phonon modes (Ω_1−Ω_5). The CdSe NPL SLs are spin-coated onto silicon oxide and measured using a 532 nm CW laser. SLs and monodispersed NPLs exhibited both characteristic first-order longitudinal optical phonon (208 cm^{-1}) and surface optical phonon (199 cm^{-1}) peaks (see Figure S18 and Table S5). However, a set of narrow peaks located below the optical phonon band was only observed in CdSe NPL SLs (Figure 3d). These modes are denoted as follows: LA_1 of 23.7 cm^{-1}, LA_2 of 41.0 cm^{-1}, LA_3 of 58.9 cm^{-1}, LA_4 of 78.5 cm^{-1}, LA_5 of 98.4 cm^{-1}, LA_6 of 106.6 cm^{-1}, and LA_7 of 117.4 cm^{-1} (summarized in Table S6). These observed values are consistent with Ω_1−Ω_5 modes with small deviations because of the limited resolution of TA measurement. These LA_1−LA_7 modes are regarded as the signatures of the ZFLAPs in the SLs.[59] Zone-folding effects transform the propagated acoustic phonons from the bulk first Brillouin zone with wave vector $\mathbf{k}_{Bulk}$ into the Raman-detectable ZFLAP with wave vector $\mathbf{k}_{SL} = \mathbf{k}_{Bulk}/N$ in the mini-Brillouin zone of SL.[60] Folding number N is experimentally calculated as 7, deduced by $N = d_0/a_0$, where SL periodicity d_0 and lattice constant a_0 are 2.85 and 0.40 nm, respectively, along the stacking direction. The zone-folding effects for optical phonon can be ignored due to the intrinsic short coherent length of optical phonon.[61,62] Bulk longitudinal acoustic phonon dispersion of wurtzite CdSe in the first Brillouin zone is calculated, as shown in Figure 3e; the inset illustrates the schematic of corresponding vibrational modes.[56] Theoretically, ZFLAP dispersion with $N = 7$ is built by implementing a linear chain model (see Supporting Information Note S5), as shown in Figure 3e. The calculated zone-center phonon modes are extracted as follows: 21.0, 41.7, 61.7, 80.9, 98.7, 114.1, and 122.2 cm^{-1}. These modes agree well with the experimental data obtained by Raman, confirming the existence of ZFLAPs.

The spatial localization of STS is illustrated in Figure 4a. For charge carrier self-trapping via coupling with acoustic phonons, the carriers are spatially localized through short-range deformation interactions. STS localization length is comparable to the length of lattice repeat unit.[63] The fwhm value of half-period of acoustic phonon wavelength (λ_a), which is written as $l_{fwhm} = 0.33\ \lambda_a$, is used to estimate the localization length of STS.[52] In our work, λ_a of ZFLAP modes is calculated as $v_l\tau = 1.67$ nm and l_{fwhm} is deduced to 0.56 nm with $v_l = 3700$ m/s in bulk CdSe and $\tau = 450$ fs from TA spectra.[64] As the schematic illustrated in Figure 4a, the STS localization length of ∼0.56 nm is approximately equal to one unit cell (∼0.40 nm) of wurtzite CdSe, suggesting that STS is highly localized. As a comparison, the coherent motion length of exciton in CdSe NPL is longer than 10 nm as reported in a previous study.[11] The strong spatial localization further relaxes the momentum conservation of STS, enabling the EPC through multiphonon participation.[65]

The energy diagram of STS is summarized in Figure 4b. Here, the EPC strength is quantified by a set of inter-related parameters [S, ΔQ, E_{ST}].[66] S is the dimensionless Huang−

https://doi.org/10.1021/acs.nanolett.0c04169
Nano Lett. 2021, 21, 4137−4144

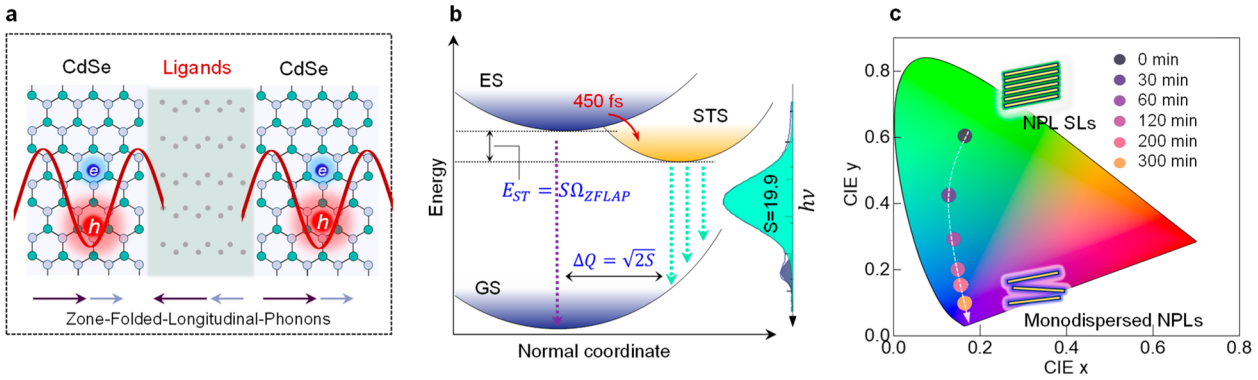

Figure 4. (a) Schematic of the STS localized via ZFLAP modes induced short-range deformation interactions. The dots between adjacent NPL layers represent the ligand chains. (b) Schematic energy diagram of STS under the normal coordinate. GS and ES are ground state and excited state, respectively. S is the Huang−Rhys parameter; E_{ST} is self-trapping energy; ΔQ represents displacement between STS and ES. (c) Continuous emission color changing during the unbundling process of CdSe NPL SLs from stacking into the monodisperse labeled in CIE chromaticity coordinates with a total duration time of 300 min.

Rhys parameter representing the average phonon number change during optical transitions,[22] ΔQ is the dimensionless displacement on normal coordinates equal to $\sqrt{2S}$ (see Supporting Information Note S6),[67] and E_{ST} is the self-trapped energy induced by acoustic modes with $E_{ST} = S\hbar\Omega$, where $\hbar\omega$ represents the average phonon energy. Among these parameters, the Huang−Rhys factor, S, plays the dominant role. The S parameter in CdSe NPL SLs is calculated to be as large as ∼19.9 (see Supporting Information Note S7). However, this value is slightly lower than that of existing STS materials, such as $Cs_2AgInCl_6$ (38.7),[25] Sb_2S_3 (38.5),[68] and NaCl (42.0)[69] but is close to that of CdSe nanoclusters (23.0).[70] However, for monodispersed NPLs the S value is only 0.1 (see Supporting Information Note S7), which is comparable to a previous report.[27] The dramatic change in S value in NPL SLs can be attributed to the following two reasons: (1) the increased phonon density of states at the mini-Brillouin zone center (Figure 3e); (2) the increased elastic strain energy concentrated in the inorganic layer (see Supporting Information Note S8, Figure S19).[71,72]

After determining the Huang−Rhys parameter, S, in CdSe NPL SLs, the recombination kinetics of STS are fully established according to the parameters set [S, ΔQ, E_{ST}], as depicted in Figure 4b. The strong EPC shifts the potential surface of the excited state upon excitation to the STS position on normal coordinate with displacement of ΔQ in a time scale of ∼450 fs. The ΔQ ($\sqrt{2S}$) reduces the wave function overlap between the ground state and STS, leading to 8.5 times longer lifetime of STS than that of exciton state (see Supporting Information Note S9). This value is consistent with the experimental result (8.3 times) obtained from TA measurements.[24] The recombination processes of STS involve energy reduction deduced by E_{ST} and multiphonon assistant deduced by S, resulting in the observed below-bandgap and broadband STS emission. Therefore, the STS emission can be well fitted by a simulated line shape determined by E_{ST} and S (Supporting Information Note S10 and Figure S20). Figure 4c presents a simple demonstration of STS manipulation via SL structure control. The sonication assistance facilitated the unbundling of CdSe NPL SLs. Thereafter, the ZFLAP modes gradually vanished, and the [S, ΔQ, E_d] continuously changed. The emission spectra, illustrated in Figure S7, can be widely tuned from green (0.22, 0.64) to blue (0.17, 0.09) in International Commission on Illumination chromaticity coordinates.

CONCLUSIONS

In summary, we demonstrated the strong STS emission from CdSe NPL SLs in the spectral range of 450−600 nm. Through comprehensive optical measurements, we revealed that STS is generated via strong coupling of excitons and zone-folded longitudinal acoustic phonons. The formation time scale of STS is ∼450 fs and the localization length is ∼0.56 nm. To evaluate the coupling strength, we estimated that the S parameter in CdSe NPL SLs is as large as ∼19.9, although its monodispersed counterpart is only ∼0.1. The increased phonon density of states at the mini-Brillouin zone center and the increased elastic strain energy concentrated in the inorganic layer are the primary reasons for the strong coupling. Our results suggest that an optimized design of the colloidal nanoplatelet structures may provide new research opportunities for EPC mechanisms and phenomenon beyond STS emission.

ASSOCIATED CONTENT

Supporting Information

The Supporting Information is available free of charge at https://pubs.acs.org/doi/10.1021/acs.nanolett.0c04169.

Detailed description of syntheses, experimental methods, additional analyses, and supporting data in experimental methods, Supporting Notes S1−S10, Figures S1−S20, and Tables S1−S6 (PDF)

AUTHOR INFORMATION

Corresponding Authors

Xinfeng Liu − *CAS Key Laboratory of Standardization and Measurement for Nanotechnology, CAS Center for Excellence in Nanoscience, National Center for Nanoscience and Technology, Beijing 100190, P.R. China; University of Chinese Academy of Sciences, Beijing 100049, P.R. China;* orcid.org/0000-0002-7662-7171; Email: liuxf@nanoctr.cn

Zhiyong Tang − *University of Chinese Academy of Sciences, Beijing 100049, P.R. China; Wenzhou Institute, University of Chinese Academy of Sciences, Wenzhou 325000, People's*

https://doi.org/10.1021/acs.nanolett.0c04169
Nano Lett. 2021, 21, 4137−4144

Republic of China; orcid.org/0000-0003-0610-0064; Email: zytang@nanoctr.cn

Authors

Xinyu Sui − *CAS Key Laboratory of Standardization and Measurement for Nanotechnology, CAS Center for Excellence in Nanoscience, National Center for Nanoscience and Technology, Beijing 100190, P.R. China; University of Chinese Academy of Sciences, Beijing 100049, P.R. China*

Xiaoqing Gao − *Wenzhou Institute, University of Chinese Academy of Sciences, Wenzhou 325000, People's Republic of China;* orcid.org/0000-0002-7718-0148

Xianxin Wu − *CAS Key Laboratory of Standardization and Measurement for Nanotechnology, CAS Center for Excellence in Nanoscience, National Center for Nanoscience and Technology, Beijing 100190, P.R. China; University of Chinese Academy of Sciences, Beijing 100049, P.R. China*

Chun Li − *CAS Key Laboratory of Standardization and Measurement for Nanotechnology, CAS Center for Excellence in Nanoscience, National Center for Nanoscience and Technology, Beijing 100190, P.R. China; University of Chinese Academy of Sciences, Beijing 100049, P.R. China; Department of Materials Science and Engineering, College of Engineering, Peking University, Beijing 100871, P.R. China*

Xuekang Yang − *University of Chinese Academy of Sciences, Beijing 100049, P.R. China; CAS Key Laboratory of Nanosystem and Hierarchical Fabrication, CAS Center for Excellence in Nanoscience, National Center for Nanoscience and Technology, Beijing 100190, P.R. China*

Wenna Du − *CAS Key Laboratory of Standardization and Measurement for Nanotechnology, CAS Center for Excellence in Nanoscience, National Center for Nanoscience and Technology, Beijing 100190, P.R. China; Key Laboratory of Semiconductor Materials Science, Beijing Key Laboratory of Low Dimensional Semiconductor Materials and Devices, Institute of Semiconductors, Chinese Academy of Sciences, Beijing 100083, China*

Zhengping Ding − *Electron Microscopy Laboratory, School of Physics, Peking University, Beijing 100871, China;* orcid.org/0000-0001-5275-5905

Shengye Jin − *State Key Laboratory of Molecular Reaction Dynamics and Collaborative Innovation Center of Chemistry for Energy Materials (iChEM), Dalian Institute of Chemical Physics, Chinese Academy of Sciences, Dalian 116023, China;* orcid.org/0000-0003-2001-2212

Kaifeng Wu − *State Key Laboratory of Molecular Reaction Dynamics and Collaborative Innovation Center of Chemistry for Energy Materials (iChEM), Dalian Institute of Chemical Physics, Chinese Academy of Sciences, Dalian 116023, China;* orcid.org/0000-0002-1047-6606

Tze Chien Sum − *Division of Physics and Applied Physics, School of Physical and Mathematical Sciences, Nanyang Technological University, Singapore 637371, Singapore;* orcid.org/0000-0003-4049-2719

Peng Gao − *Electron Microscopy Laboratory, School of Physics, Peking University, Beijing 100871, China;* orcid.org/0000-0003-0860-5525

Junjie Liu − *State Key Laboratory for Turbulence and Complex System, Department of Mechanics and Engineering Science, College of Engineering and Beijing Innovation Center for Engineering Science and Advanced Technology, Peking University, Beijing 100871, P.R. China*

Xiaoding Wei − *State Key Laboratory for Turbulence and Complex System, Department of Mechanics and Engineering Science, College of Engineering and Beijing Innovation Center for Engineering Science and Advanced Technology, Peking University, Beijing 100871, P.R. China;* orcid.org/0000-0002-5173-4923

Jun Zhang − *State Key Laboratory of Superlattices and Microstructures, Institute of Semiconductors, and Center of Materials Science and Optoelectronics Engineering, Chinese Academy of Sciences, Beijing 100083, China;* orcid.org/0000-0002-9831-6796

Qing Zhang − *Department of Materials Science and Engineering, College of Engineering, Peking University, Beijing 100871, P.R. China;* orcid.org/0000-0002-6869-0381

Complete contact information is available at: https://pubs.acs.org/10.1021/acs.nanolett.0c04169

Author Contributions

X.L designed and supervised the research. X.G synthesized and provided the sample. X.S. performed the TA measurements and data analysis. X.W performed the steady-state low-frequency Raman spectroscopy. X.Y. performed the SAXS measurements. Z.D. and P.G. performed the HADDF imaging. All the authors wrote and revised the manuscript.

Notes

The authors declare no competing financial interest.

■ ACKNOWLEDGMENTS

X.F.L. thanks the support of the Strategic Priority Research Program of Chinese Academy of Sciences (XDB36000000), the Ministry of Science and Technology (2016YFA0200700 and 2017YFA0205004), the CAS Instrument Development Project (No. Y950291), the National Natural Science Foundation of China (61704038, 21673054, and 11874130) and Open Research Fund Program of the State Key Laboratory of Low-Dimensional Quantum Physics (KF201902). Q.Z. is grateful for funding support from the Ministry of Science and Technology (2017YFA0205700; 2017YFA0304600), the National Natural Science Foundation of China (61774003 and 61521004). J.Z. acknowledges support from Beijing Natural Science Foundation (JQ18014), the National Basic Research Program of China (2016YFA0301200 and 2017YFA0303401). This work was also supported by the National Natural Science Foundation of China (61307120, 61704038, 12074086, 21805188, and 11474187).

■ REFERENCES

(1) Son, J. S.; Wen, X. D.; Joo, J.; Chae, J.; Baek, S. I.; Park, K.; Kim, J. H.; An, K.; Yu, J. H.; Kwon, S. G.; Choi, S. H.; Wang, Z.; Kim, Y. W.; Kuk, Y.; Hoffmann, R.; Hyeon, T. Large-scale soft colloidal template synthesis of 1.4 nm thick CdSe nanosheets. *Angew. Chem., Int. Ed.* **2009**, *48*, 6861−6864.

(2) Son, J. S.; Yu, J. H.; Kwon, S. G.; Lee, J.; Joo, J.; Hyeon, T. Colloidal synthesis of ultrathin two-dimensional semiconductor nanocrystals. *Adv. Mater.* **2011**, *23*, 3214−3219.

(3) Ithurria, S.; Tessier, M. D.; Mahler, B.; Lobo, R. P.; Dubertret, B.; Efros, A. L. Colloidal nanoplatelets with two-dimensional electronic structure. *Nat. Mater.* **2011**, *10*, 936−941.

(4) Joo, J.; Son, J. S.; Kwon, S. G.; Yu, J. H.; Hyeon, T. Low-temperature solution-phase synthesis of quantum well structured CdSe nanoribbons. *J. Am. Chem. Soc.* **2006**, *128*, 5632−5633.

(5) Ji, B.; Rabani, E.; Efros, A. L.; Vaxenburg, R.; Ashkenazi, O.; Azulay, D.; Banin, U.; Millo, O. Dielectric Confinement and Excitonic

Effects in Two-Dimensional Nanoplatelets. *ACS Nano* **2020**, *14*, 8257−8265.
(6) Movilla, J. L.; Planelles, J.; Climente, J. I. Dielectric Confinement Enables Molecular Coupling in Stacked Colloidal Nanoplatelets. *J. Phys. Chem. Lett.* **2020**, *11*, 3294−3300.
(7) Guzelturk, B.; Pelton, M.; Olutas, M.; Demir, H. V. Giant Modal Gain Coefficients in Colloidal II-VI Nanoplatelets. *Nano Lett.* **2019**, *19*, 277−282.
(8) Altintas, Y.; Gungor, K.; Gao, Y.; Sak, M.; Quliyeva, U.; Bappi, G.; Mutlugun, E.; Sargent, E. H.; Demir, H. V. Giant Alloyed Hot Injection Shells Enable Ultralow Optical Gain Threshold in Colloidal Quantum Wells. *ACS Nano* **2019**, *13*, 10662−10670.
(9) Erdem, O.; Foroutan, S.; Gheshlaghi, N.; Guzelturk, B.; Altintas, Y.; Demir, H. V. Thickness-Tunable Self-Assembled Colloidal Nanoplatelet Films Enable Ultrathin Optical Gain Media. *Nano Lett.* **2020**, *20*, 6459−6465.
(10) Liu, Y. H.; Wayman, V. L.; Gibbons, P. C.; Loomis, R. A.; Buhro, W. E. Origin of high photoluminescence efficiencies in CdSe quantum belts. *Nano Lett.* **2010**, *10*, 352−357.
(11) Li, Q.; Lian, T. Exciton Spatial Coherence and Optical Gain in Colloidal Two-Dimensional Cadmium Chalcogenide Nanoplatelets. *Acc. Chem. Res.* **2019**, *52*, 2684−2693.
(12) Grim, J. Q.; Christodoulou, S.; Di Stasio, F.; Krahne, R.; Cingolani, R.; Manna, L.; Moreels, I. Continuous-wave biexciton lasing at room temperature using solution-processed quantum wells. *Nat. Nanotechnol.* **2014**, *9*, 891−895.
(13) She, C.; Fedin, I.; Dolzhnikov, D. S.; Demortiere, A.; Schaller, R. D.; Pelton, M.; Talapin, D. V. Low-threshold stimulated emission using colloidal quantum wells. *Nano Lett.* **2014**, *14*, 2772−2777.
(14) She, C.; Fedin, I.; Dolzhnikov, D. S.; Dahlberg, P. D.; Engel, G. S.; Schaller, R. D.; Talapin, D. V. Red, yellow, green, and blue amplified spontaneous emission and lasing using colloidal CdSe nanoplatelets. *ACS Nano* **2015**, *9*, 9475−9485.
(15) Scott, R.; Heckmann, J.; Prudnikau, A. V.; Antanovich, A.; Mikhailov, A.; Owschimikow, N.; Artemyev, M.; Climente, J. I.; Woggon, U.; Grosse, N. B.; Achtstein, A. W. Directed emission of CdSe nanoplatelets originating from strongly anisotropic 2D electronic structure. *Nat. Nanotechnol.* **2017**, *12*, 1155−1160.
(16) Gao, Y. N.; Weidman, M. C.; Tisdale, W. A. CdSe Nanoplatelet Films with Controlled Orientation of their Transition Dipole Moment. *Nano Lett.* **2017**, *17*, 3837−3843.
(17) Ma, X.; Diroll, B. T.; Cho, W.; Fedin, I.; Schaller, R. D.; Talapin, D. V.; Wiederrecht, G. P. Anisotropic Photoluminescence from Isotropic Optical Transition Dipoles in Semiconductor Nanoplatelets. *Nano Lett.* **2018**, *18*, 4647−4652.
(18) Panfil, Y. E.; Oded, M.; Banin, U. Colloidal Quantum Nanostructures: Emerging Materials for Display Applications. *Angew. Chem., Int. Ed.* **2018**, *57*, 4274−4295.
(19) Zhao, J.; Zhao, W.; Du, W.; Su, R.; Xiong, Q. Dynamics of exciton energy renormalization in monolayer transition metal disulfides. *Nano Res.* **2020**, *13*, 1399−1405.
(20) Panfil, Y. E.; Oded, M.; Banin, U. Kolloidale Quantennanostrukturen: neue Materialien für Displayanwendungen. *Angew. Chem.* **2018**, *130*, 4354−4376.
(21) Landau, L. D. Electron motion in crystal lattices. *Phys. Z. Sowjet.* **1933**, *3*, 664.
(22) Song, K.; Williams, R. T. *Self-trapped excitons*, 2nd ed.; Springer Science & Business Media: Verlag Berlin Heidelberg, 1996; Vol. *105*.
(23) Singh, J. *Excitation energy transfer processes in condensed matter: theory and applications*, 1st ed.; Springer Science & Business Media: New York, 1994.
(24) Smith, M. D.; Karunadasa, H. I. White-Light Emission from Layered Halide Perovskites. *Acc. Chem. Res.* **2018**, *51*, 619−627.
(25) Luo, J.; Wang, X.; Li, S.; Liu, J.; Guo, Y.; Niu, G.; Yao, L.; Fu, Y.; Gao, L.; Dong, Q.; Zhao, C.; Leng, M.; Ma, F.; Liang, W.; Wang, L.; Jin, S.; Han, J.; Zhang, L.; Etheridge, J.; Wang, J.; Yan, Y.; Sargent, E. H.; Tang, J. Efficient and stable emission of warm-white light from lead-free halide double perovskites. *Nature* **2018**, *563*, 541−545.
(26) Dong, S.; Lian, J.; Jhon, M. H.; Chan, Y.; Loh, Z. H. Pump-Power Dependence of Coherent Acoustic Phonon Frequencies in Colloidal CdSe/CdS Core/Shell Nanoplatelets. *Nano Lett.* **2017**, *17*, 3312−3319.
(27) Maddux, C. J. A.; Kelley, D. F.; Kelley, A. M. Weak Exciton−Phonon Coupling in CdSe Nanoplatelets from Quantitative Resonance Raman Intensity Analysis. *J. Phys. Chem. C* **2018**, *122*, 27100−27106.
(28) Salvador, M. R.; Graham, M. W.; Scholes, G. D. Exciton-phonon coupling and disorder in the excited states of CdSe colloidal quantum dots. *J. Chem. Phys.* **2006**, *125*, 184709.
(29) Jethi, L.; Mack, T. G.; Kambhampati, P. Extending Semiconductor Nanocrystals from the Quantum Dot Regime to the Molecular Cluster Regime. *J. Phys. Chem. C* **2017**, *121*, 26102−26107.
(30) Mack, T. G.; Jethi, L.; Kambhampati, P. Strategy for Exploiting Self-Trapped Excitons in Semiconductor Nanocrystals for White Light Generation. *ACS Photonics* **2019**, *6*, 1118−1124.
(31) Bowers, M. J., 2nd; McBride, J. R.; Rosenthal, S. J. White-light emission from magic-sized cadmium selenide nanocrystals. *J. Am. Chem. Soc.* **2005**, *127*, 15378−15379.
(32) Bowers, M. J., 2nd; McBride, J. R.; Garrett, M. D.; Sammons, J. A.; Dukes, A. D., 3rd; Schreuder, M. A.; Watt, T. L.; Lupini, A. R.; Pennycook, S. J.; Rosenthal, S. J. Structure and ultrafast dynamics of white-light-emitting CdSe nanocrystals. *J. Am. Chem. Soc.* **2009**, *131*, 5730−5731.
(33) Sung, S. H.; Schnitzer, N.; Brown, L.; Park, J.; Hovden, R. Stacking, strain, and twist in 2D materials quantified by 3D electron diffraction. *Physical Review Materials* **2019**, *3*, 064003.
(34) Babayan, Y.; Barton, J. E.; Greyson, E. C.; Odom, T. W. Templated and hierarchical assembly of CdSe/ZnS quantum dots. *Adv. Mater.* **2004**, *16*, 1341−1345.
(35) Zhao, Y.; Luo, X.; Li, H.; Zhang, J.; Araujo, P. T.; Gan, C. K.; Wu, J.; Zhang, H.; Quek, S. Y.; Dresselhaus, M. S.; Xiong, Q. Interlayer breathing and shear modes in few-trilayer MoS_2 and WSe_2. *Nano Lett.* **2013**, *13*, 1007−1015.
(36) Abecassis, B. Three-Dimensional Self Assembly of Semiconducting Colloidal Nanocrystals: From Fundamental Forces to Collective Optical Properties. *ChemPhysChem* **2016**, *17*, 618−631.
(37) Courty, A.; Mermet, A.; Albouy, P. A.; Duval, E.; Pileni, M. P. Vibrational coherence of self-organized silver nanocrystals in f.c.c. supra-crystals. *Nat. Mater.* **2005**, *4*, 395−398.
(38) Zanjani, M. B.; Lukes, J. R. Phonon dispersion and thermal conductivity of nanocrystal superlattices using three-dimensional atomistic models. *J. Appl. Phys.* **2014**, *115*, 143515.
(39) Lisiecki, I.; Halté, V.; Petit, C.; Pileni, M.-P.; Bigot, J.-Y. Vibration Dynamics of Supra-Crystals of Cobalt Nanocrystals Studied With Femtosecond Laser Pulses. *Adv. Mater.* **2008**, *20*, 4176−4179.
(40) Lisiecki, I.; Polli, D.; Yan, C.; Soavi, G.; Duval, E.; Cerullo, G.; Pileni, M. P. Coherent longitudinal acoustic phonons in three-dimensional supracrystals of cobalt nanocrystals. *Nano Lett.* **2013**, *13*, 4914−4919.
(41) Poyser, C. L.; Czerniuk, T.; Akimov, A.; Diroll, B. T.; Gaulding, E. A.; Salasyuk, A. S.; Kent, A. J.; Yakovlev, D. R.; Bayer, M.; Murray, C. B. Coherent Acoustic Phonons in Colloidal Semiconductor Nanocrystal Superlattices. *ACS Nano* **2016**, *10*, 1163−1169.
(42) Guo, P.; Stoumpos, C. C.; Mao, L.; Sadasivam, S.; Ketterson, J. B.; Darancet, P.; Kanatzidis, M. G.; Schaller, R. D. Cross-plane coherent acoustic phonons in two-dimensional organic-inorganic hybrid perovskites. *Nat. Commun.* **2018**, *9*, 2019.
(43) Gao, X.; Zhang, X.; Zhao, L.; Huang, P.; Han, B.; Lv, J.; Qiu, X.; Wei, S. H.; Tang, Z. Distinct Excitonic Circular Dichroism between Wurtzite and Zincblende CdSe Nanoplatelets. *Nano Lett.* **2018**, *18*, 6665−6671.
(44) Salem, L. Attractive forces between long saturated chains at short distances. *J. Chem. Phys.* **1962**, *37*, 2100−2113.
(45) Pollard, W. T.; Lee, S. Y.; Mathies, R. A. Wave packet theory of dynamic absorption spectra in femtosecond pump−probe experiments. *J. Chem. Phys.* **1990**, *92*, 4012−4029.

https://doi.org/10.1021/acs.nanolett.0c04169
Nano Lett. 2021, 21, 4137−4144

(46) Sasajima, Y.; Tanimura, K. Optical transitions of self-trapped holes in amorphous SiO_2. *Phys. Rev. B: Condens. Matter Mater. Phys.* **2003**, *68*, 014204.
(47) Sootha, G.; Padam, G.; Gupta, S. Electron and hole trapped centres in CdS. *physica status solidi (a)* **1980**, *60*, 599−606.
(48) Dimmock, J. O.; Wheeler, R. G. Exciton Structure and Zeeman Effects in Cadmium Selenide. *J. Appl. Phys.* **1961**, *32*, 2271−2277.
(49) Dexheimer, S. L.; Van Pelt, A. D.; Brozik, J. A.; Swanson, B. I. Femtosecond vibrational dynamics of self-trapping in a quasi-one-dimensional system. *Phys. Rev. Lett.* **2000**, *84*, 4425−4428.
(50) Morrissey, F. X.; Dexheimer, S. L. Vibrational spectroscopy of structurally relaxed self-trapped excitons via excited-state resonant impulsive stimulated Raman spectroscopy. *J. Phys. Chem. B* **2012**, *116*, 10582−10589.
(51) Mance, J. G.; Felver, J. J.; Dexheimer, S. L. Optical and Acoustic Phonon Dynamics of Exciton Self-Trapping in a Non-degenerate Quasi-One-Dimensional Charge Density Wave System. *J. Phys. Chem. C* **2014**, *118*, 11186−11192.
(52) Morrissey, F. X.; Dexheimer, S. L. Coherent acoustic phonon generation in exciton self-trapping. *Phys. Rev. B: Condens. Matter Mater. Phys.* **2010**, *81*, 094302.
(53) Li, Q.; Lian, T. Area- and Thickness-Dependent Biexciton Auger Recombination in Colloidal CdSe Nanoplatelets: Breaking the ″Universal Volume Scaling Law″. *Nano Lett.* **2017**, *17*, 3152−3158.
(54) Prabhu, S. S.; Vengurlekar, A. S.; Roy, S. K.; Shah, J. Nonequilibrium dynamics of hot carriers and hot phonons in CdSe and GaAs. *Phys. Rev. B: Condens. Matter Mater. Phys.* **1995**, *51*, 14233−14246.
(55) Pelton, M.; Ithurria, S.; Schaller, R. D.; Dolzhnikov, D. S.; Talapin, D. V. Carrier cooling in colloidal quantum wells. *Nano Lett.* **2012**, *12*, 6158−6163.
(56) Widulle, F.; Kramp, S.; Pyka, N. M.; Gobel, A.; Ruf, T.; Debernardi, A.; Lauck, R.; Cardona, M. The phonon dispersion of wurtzite CdSe. *Phys. B* **1999**, *263*, 448−451.
(57) Batignani, G.; Fumero, G.; Srimath Kandada, A. R.; Cerullo, G.; Gandini, M.; Ferrante, C.; Petrozza, A.; Scopigno, T. Probing femtosecond lattice displacement upon photo-carrier generation in lead halide perovskite. *Nat. Commun.* **2018**, *9*, 1971.
(58) Trallero-Giner, C.; Debernardi, A.; Cardona, M.; Menendez-Proupin, E.; Ekimov, A. I. Optical vibrons in CdSe dots and dispersion relation of the bulk material. *Phys. Rev. B: Condens. Matter Mater. Phys.* **1998**, *57*, 4664−4669.
(59) Ionov, R. I. Folded Acoustic Phonons in Amorphous SeTe/CdSe Superlattices. *Europhysics Letters (EPL)* **1992**, *19*, 317−322.
(60) Bartels, A.; Dekorsy, T.; Kurz, H.; Köhler, K. Coherent Zone-Folded Longitudinal Acoustic Phonons in Semiconductor Superlattices: Excitation and Detection. *Phys. Rev. Lett.* **1999**, *82*, 1044−1047.
(61) Santos, P.; Hundhausen, M.; Ley, L. Observation of folded-zone acoustical phononS by Raman scattering in amorphous Si-SiN x superlattices. *Phys. Rev. B: Condens. Matter Mater. Phys.* **1986**, *33*, 1516.
(62) Chen, C.; Chen, Y.; Shih, A.; Lee, S.; Jiang, H. Zone-folding effect on optical phonon in $GaN/Al_{0.2}Ga_{0.8}N$ superlattices. *Appl. Phys. Lett.* **2001**, *78*, 3035−3037.
(63) Toyozawa, Y. Self-trapping of an electron by the acoustical mode of lattice vibration. *Prog. Theor. Phys.* **1961**, *26*, 29−44.
(64) Saviot, L.; Champagnon, B.; Duval, E.; Kudriavtsev, I. A.; Ekimov, A. I. Size dependence of acoustic and optical vibrational modes of CdSe nanocrystals in glasses. *J. Non-Cryst. Solids* **1996**, *197*, 238−246.
(65) Huang, K.; Rhys, A. Theory of light absorption and non-radiative transitions in F-centres. *Proceedings of the Royal Society of London. Series A. Mathematical and Physical Sciences* **1950**, *204*, 406−423.
(66) Wu, B.; Ning, W.; Xu, Q.; Manjappa, M.; Feng, M.; Ye, S.; Fu, J.; Lie, S.; Yin, T.; Wang, F.; Goh, T. W.; Harikesh, P. C.; Tay, Y. K. E.; Shen, Z. X.; Huang, F.; Singh, R.; Zhou, G.; Gao, F.; Sum, T. C. Strong self-trapping by deformation potential limits photovoltaic performance in bismuth double perovskite. *Sci. Adv.* **2021**, *7*, eabd3160.
(67) Smith, M. D.; Jaffe, A.; Dohner, E. R.; Lindenberg, A. M.; Karunadasa, H. I. Structural origins of broadband emission from layered Pb-Br hybrid perovskites. *Chem. Sci.* **2017**, *8*, 4497−4504.
(68) Yang, Z.; Wang, X.; Chen, Y.; Zheng, Z.; Chen, Z.; Xu, W.; Liu, W.; Yang, Y. M.; Zhao, J.; Chen, T.; Zhu, H. Ultrafast self-trapping of photoexcited carriers sets the upper limit on antimony trisulfide photovoltaic devices. *Nat. Commun.* **2019**, *10*, 4540.
(69) Lemos, A. M.; Markham, J. J. Calculation of the Huang-Rhys factor for F-centers. *J. Phys. Chem. Solids* **1965**, *26*, 1837−1851.
(70) Mooney, J.; Krause, M. M.; Saari, J. I.; Kambhampati, P. Challenge to the deep-trap model of the surface in semiconductor nanocrystals. *Phys. Rev. B: Condens. Matter Mater. Phys.* **2013**, *87*, 081201.
(71) Ma, Z.; Liu, Z.; Lu, S.; Wang, L.; Feng, X.; Yang, D.; Wang, K.; Xiao, G.; Zhang, L.; Redfern, S. A. T.; Zou, B. Pressure-induced emission of cesium lead halide perovskite nanocrystals. *Nat. Commun.* **2018**, *9*, 4506.
(72) Sato, K.; Saito, R.; Cong, C.; Yu, T.; Dresselhaus, M. S. Zone folding effect in Raman G-band intensity of twisted bilayer graphene. *Phys. Rev. B: Condens. Matter Mater. Phys.* **2012**, *86*, 125414.

https://doi.org/10.1021/acs.nanolett.0c04169
Nano Lett. 2021, 21, 4137−4144